

## Accurate electron affinity of Ti and fine structures of its anions

Rulin Tang, Xiaoxi Fu, and Chuangang Ning

Citation: *The Journal of Chemical Physics* **149**, 134304 (2018); doi: 10.1063/1.5049629

View online: <https://doi.org/10.1063/1.5049629>

View Table of Contents: <http://aip.scitation.org/toc/jcp/149/13>

Published by the *American Institute of Physics*

---

---

**PHYSICS TODAY**

WHITEPAPERS

### ADVANCED LIGHT CURE ADHESIVES

Take a closer look at what these environmentally friendly adhesive systems can do

READ NOW

PRESENTED BY  
 **MASTERBOND**  
ADHESIVES | SEALANTS | COATINGS

## Accurate electron affinity of Ti and fine structures of its anions

Rulin Tang,<sup>1</sup> Xiaoxi Fu,<sup>1</sup> and Chuangang Ning<sup>1,2,a)</sup>

<sup>1</sup>Department of Physics, State Key Laboratory of Low-Dimensional Quantum Physics, Tsinghua University, Beijing 10084, China

<sup>2</sup>Collaborative Innovation Center of Quantum Matter, Beijing, China

(Received 24 July 2018; accepted 17 September 2018; published online 2 October 2018)

The high-resolution photoelectron energy spectra of atomic titanium and its hydride anions were obtained on a slow-electron velocity-map imaging spectrometer equipped with a cold ion trap. The cold ion trap employed in the present measurement was found to be very helpful for reducing the interference from the titanium hydride anions. The electron affinity of Ti was determined to be 609.29(34) cm<sup>-1</sup> or 75.54(4) meV. The accuracy was improved by a factor of 350 compared with the previous result. The fine structures of Ti<sup>-</sup> were clearly resolved: 70.0(12)(<sup>4</sup>F<sub>5/2</sub>), 165.2(15)(<sup>4</sup>F<sub>7/2</sub>), and 285.2(15) cm<sup>-1</sup> (<sup>4</sup>F<sub>9/2</sub>) above its ground state <sup>4</sup>F<sub>3/2</sub>. Moreover, the measured electron affinity and vibrational frequency of TiH can be reproduced well using the high level calculations. *Published by AIP Publishing.* <https://doi.org/10.1063/1.5049629>

### I. INTRODUCTION

Titanium has excellent physical, chemical, mechanical, and biological properties. The highest strength-to-density ratio in the metallic elements, along with high corrosion resistance, high fatigue resistance, and high melting point, makes titanium and its alloys widely used in aircraft, naval ships, spacecraft, and missiles. Titanium is biocompatible and is the primary material of some surgical implement and implants. Moreover, titania (TiO<sub>2</sub>) is an important semiconducting material with widespread applications in photovoltaics,<sup>1-4</sup> pollution management,<sup>5</sup> and heterogeneous catalysis.<sup>6-8</sup> These magical properties are closely related to the unique electronic structure of the Ti atom. In contrast to the extensive studies and widespread applications of titanium and titania,<sup>9-13</sup> our knowledge is rather limited with the atomic anion Ti<sup>-</sup>. For example, electron affinity (EA) is a fundamental parameter of an element, which measures the capability of an atom to form the corresponding negative ion. EAs of most elements have been accurately measured with an accuracy of ~0.1 meV.<sup>14-16</sup> However, the best reported EA value of Ti is 80 meV with a large uncertainty of ±14 meV.<sup>17</sup> Here, we present the high-resolution photoelectron spectra of the Ti<sup>-</sup> anion in order to measure its EA and fine structures with high accuracy.

The EA values are mainly measured using the photoelectron spectroscopy of anions. That is, an electron in an anion A<sup>-</sup> is detached by a photon: A<sup>-</sup> + hν = A + e<sup>-</sup>. Given the photon energy hν and the measured kinetic energy of the outgoing electron eKE, the EA is derived by a simple relation: EA = hν - eKE. Generally, there are four experimental methods for EA measurements: laser photoelectron spectroscopy (LPES), laser photodetachment threshold (LPT), laser photodetachment microscope (LPM), and slow-electron

velocity-map imaging (SEVI). A majority of primal EAs of elements were obtained with uncertainty around 10 meV by Lineberger and co-workers in 1970s and 1980s.<sup>17-19</sup> The semi-spherical analyzer used for measuring the kinetic energy of electrons is the bottleneck of this method. Later, many EA values were updated by Haugen and co-workers via the LPT method.<sup>16,20</sup> The total photodetachment cross section σ is proportional to eKE'<sup>l'+1/2</sup> according to the Wigner threshold law,<sup>21</sup> where l' is the angular quantum number of the outgoing photoelectron. The LPT method scans the photon energy while recording the cross section σ at the same time. Obviously, when hν < EA, σ should be zero, and there is an onset of σ near the threshold hν = EA as hν increases. This method provides an accurate approach to the EA measurement for an s-wave detachment as the onset is quite sharp. By contrast, when it comes to a transition element where a p-wave detachment usually occurs, this method becomes less reliable due to a zero-slope onset near the threshold. In addition, the transition element atoms usually have complicated electronic structures, especially the excited states of anions, which makes the situation even worse. The ability of LPT to resolve the congested photodetachment channels is rather limited due to the zero-slope onset.<sup>22</sup> Therefore, the LPT method is more suitable to measure EAs of main-group elements than transition elements. Several late transition elements were measured using this method, such as Cu<sup>23</sup> and Pt.<sup>15</sup> Another method, LPM, was established recently by Blondel and co-workers.<sup>24-26</sup> The eKE is measured through the interference patterns of electrons. This method is able to obtain the most accurate EA values by far, usually with 0.01 cm<sup>-1</sup> uncertainty, for example, <sup>16</sup>O 11 784.676(7),<sup>27</sup> <sup>32</sup>S 16 752.975 3(41),<sup>28</sup> and Ge 9942.206(10).<sup>29</sup> However, to observe a clear interference pattern, eKE must be lower than 1 cm<sup>-1</sup>. At such a low electron kinetic energy, only s-wave detachment has a large enough photodetachment cross section. For this reason, the LPM method is also limited to the main-group element. Recently,

<sup>a)</sup>Electronic mail: ningcg@tsinghua.edu.cn

our group has measured EAs of a few transition metal elements via the SEVI method. SEVI has a very impressive energy resolution for electrons with a low kinetic energy, which was originally developed by the Neumark group to resolve the electronic and vibrational structures of molecular anions.<sup>30–34</sup> With SEVI, EAs of several transition elements have been improved to  $\sim 0.5$   $\text{cm}^{-1}$  uncertainties by our group,<sup>14,22,35–40</sup> such as Zr 3494.67(72)  $\text{cm}^{-1}$ , Nb 7399.35(50)  $\text{cm}^{-1}$ , and Re 487.13(51)  $\text{cm}^{-1}$ .

The ground state of  $\text{Ti}^-$  is  $3d^34s^2^4F_{3/2}$ . It has three fine-structure bound excited states, i.e.,  $J = 5/2$ ,  $7/2$ , and  $9/2$ . The EA value of Ti was first reported to be 80(14) meV by Feigler *et al.* utilizing the LPES method in 1981.<sup>17</sup> The fine-structure splittings were not resolved but were estimated to be 72(7)  $\text{cm}^{-1}$ , 171(12)  $\text{cm}^{-1}$ , 295(15)  $\text{cm}^{-1}$  via the linear iso-electronic extrapolation.<sup>17,41</sup> In 1987, Ilin *et al.* reported its EA as 87(7) meV using the electric field detachment method.<sup>42</sup> Later, Liu *et al.* studied the photoelectron spectra of  $\text{Ti}_n^-$  ( $n = 1–130$ ) clusters with a similar energy resolution.<sup>43</sup>

The prerequisite for measuring EA of an element is to generate the corresponding negative ions. The  $\text{Ti}^-$  anion beam is usually very weak in a laser ablation ion source due to the low EA value of Ti. The situation becomes even worse due to the contamination of titanium hydride anion  $\text{TiH}^-$ . The intensity of  $\text{TiH}^-$  is much stronger than that of  $\text{Ti}^-$ . No indications are observed that the hydride negative ion signals become weaker after a prolonged laser ablation, presumably due to the high reactivity of titanium with the small mass hydrogen atoms, which can easily diffuse into the metal lattice. The other possible source of hydrogen is the residual  $\text{H}_2$  in the vacuum chamber, which can react immediately with the fresh surface created by the laser ablation. Actually, titanium is the working medium of titanium sublimation pumps for absorbing  $\text{H}_2$ . Titanium has five stable isotopes  $^{46}\text{Ti}$  (8.25%),  $^{47}\text{Ti}$  (7.44%),  $^{48}\text{Ti}$  (73.72%),  $^{49}\text{Ti}$  (5.41%), and  $^{50}\text{Ti}$  (5.18%). In our mass spectra, the dominant composition of anions with a mass  $m = 48$  is  $^{47}\text{TiH}^-$ . The anion  $m = 46$  is pure  $\text{Ti}^-$ , but it is too weak to achieve a high statistic accuracy. The negative ions produced by laser ablation are usually quite hot. The thermal broadening and hot bands make the energy spectra of molecular anions almost a continuous distribution, which overlaps with the energy spectra of atomic anions. Consequently,

the signal-to-noise ratio is not good enough for an accurate measurement. The situation frequently happened in our previous experiments for the early transition metal elements. One solution to the hydride contamination is a cryogenically cold ion trap, which can make the energy spectra of molecular anions clean and sharp. As demonstrated recently, we successfully measured the EA of hafnium using the cryo-SEVI method.<sup>40</sup> Hafnium is a heavy element in the same group as titanium. Similar to titanium, hafnium also has a significant hydride contamination problem.

In the present work, we first describe our cryo-SEVI apparatus in detail and then use it to improve the accuracy of the EA of Ti to the sub- $\text{cm}^{-1}$  accuracy.

## II. EXPERIMENTAL SETUP

Compared with our first-generation apparatus, the main improvement of our second-generation machine is the cryogenic ion trap. The detailed description of the first-generation apparatus can be found in our previous studies.<sup>39</sup> Figure 1 shows the schematic diagram of the second-generation machine. It has four major sections: a laser ablation source, a cryogenic ion trap,<sup>44,45</sup> a Wiley-McLaren type time-of-flight (TOF) mass spectrometer,<sup>46</sup> and a photoelectron velocity-map imaging (VMI) system.<sup>47,48</sup> The apparatus runs at 20-Hz repetition rate. Anions are generated by focusing a laser beam onto a translating and rotating metal disk. The ablation laser is the second-harmonic output of a Nd:YAG laser (532 nm,  $\sim 10$  mJ/pulse). The generated ions fly through an Einzel lens and are accumulated in an ion trap. The ion trap is filled with the buffer gas (He 80%,  $\text{H}_2$  20%). The anions lose their kinetic energy through collisions with buffer gas and are confined radially by a suit of linear radio frequency (RF) octupole and axially by two electrodes at the entrance and the exit. The frequency of our homemade RF power can be tuned from 0.9 MHz to 3.1 MHz. The amplitude of RF can be adjusted from 50 V to 1000 V (peak to peak). 1.3 MHz is routinely used for heavy anions ( $m > 100$ ), and 3.1 MHz is used for light anions ( $m < 100$ ). The ion trap is mounted on the second stage of a liquid helium refrigerator (SHI Cryogenics Group, F-50). It can reach 5 K temperature in around an hour. A 40-K copper shield in contact with the first stage of the

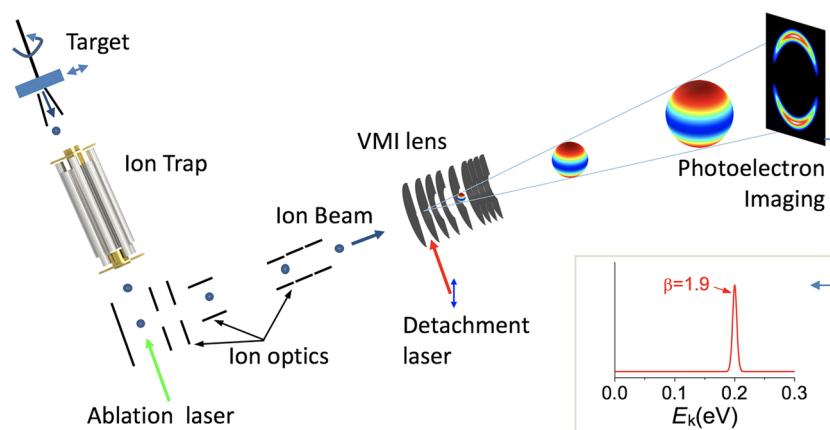


FIG. 1. Schematic view of our cryo-SEVI apparatus. The mass gate and the ion detector before the VMI lens are not shown.

refrigerator is used to isolate the ion trap from the thermal radiation of the surrounding environment. One silicon diode thermometer (Lake Shore, DT-670C-CU) and two heating resistances (Lake Shore, HTR-25) are attached on the wall of the ion trap, which can control the ion trap at any temperature between 5 and 300 K with a temperature controller (Sandford Research System, CTC100). The ions are usually stored in the ion trap for 45 ms. The internal freedoms of ions can be effectively thermalized through collisions with the buffer gas. The operating temperature is usually set to 15 K in order to avoid condensation of  $\text{H}_2$ . It can run at the lowest temperature 5 K for several hours without serious condensation of  $\text{H}_2$ . Considering the RF heating effect, the real temperature of ions may be slightly higher than the nominal temperature. After stored for up to 45 ms, the ions are extracted and focused into the TOF mass spectrometer, where they are accelerated by a  $-1000$  V high-voltage pulse. The ions are detected by an ion detector with a pair of micro-channel plates. The ion detector can be rotated away from the ion flight path as for the subsequent photodetachment experiment. Because the ion trap provides temporally and spatially more compact ion packets, the mass resolution ( $m/\Delta m$ ) is improved greatly from 300 to 1000 for  $m \sim 200$ . The anions of interest are selected out via a mass gate and then photodetached in the interaction zone of the VMI system. The detachment laser is from a Spectra-Physics dye laser system (400–920 nm, linewidth  $0.06 \text{ cm}^{-1}$ ) pumped by the Quanta-Ray Pro 290 Nd:YAG laser (20 Hz, 400 mJ/pulse at 532 nm). The linearly polarized laser beam intersects with the anion beam orthogonally. The outgoing photoelectrons with the same kinetic energy form an expanding spherical shell. The photoelectron shell is projected onto a home-built phosphor screen by the electric field of the VMI system. A pair of microchannel plates is used to enhance the phosphor screen.

The phosphor screen of our new machine has a larger sensitive area (80 mm in diameter), which significantly extends the measurement range of photoelectrons kinetic energy. The raw photoelectron images are captured in real time frame by frame via a CCD camera, and the hitting position of each photoelectron is recorded in the event-counting mode. Typically, a photoelectron image is an accumulated result of 50 000–200 000 laser shots. The wavelength of the dye laser is continuously monitored by a HighFinesse WS6-600 wavelength meter with an accuracy of  $0.02 \text{ cm}^{-1}$ . The polarization vector of the detachment laser is parallel to the phosphor screen. Therefore, the imaging system has a cylindrical symmetry. The 3D photoelectron shell can be reconstructed from the projected 2D image. In the present work, the maximum entropy velocity Legendre reconstruction (MEVELER) method<sup>49</sup> is used. The kinetic energy of photoelectrons  $eKE$  is proportional to the square of the radius of shell  $r$ , i.e.,  $eKE = \alpha r^2$ . The coefficient  $\alpha$  can be determined via the energy calibration procedure, which is usually done by measuring atomic anions with known energy levels or by varying the photon energy  $h\nu$ .

To test the cold ion trap, we acquired the energy spectra of  $\text{ZrO}_2^-$  at  $h\nu = 13\,539.14 \text{ cm}^{-1}$  at room temperature 300 K and at a low temperature 15 K, respectively. As Fig. 2 shows, the cold ion trap can effectively eliminate hot bands of anions at 15 K. Moreover, the remaining two peaks become much narrower because of the less population on the rotationally excited state of ions. Our result for  $\text{ZrO}_2^-$  is consistent with that reported by Kim *et al.* recently.<sup>10</sup> This ability to cool molecular ions to  $\sim 10$  K temperature is very helpful for the EA measurement of Ti in the present work. Moreover, the ion trap can accumulate the anion beam to enhance its intensity. This is an important feature for the anions with a low EA value.

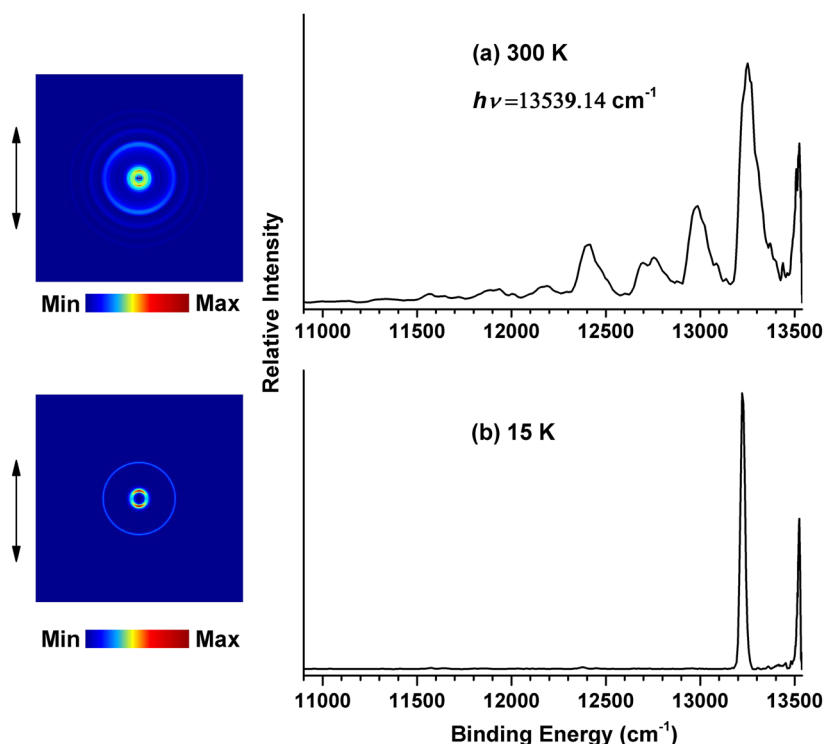


FIG. 2. Comparison of photoelectron images and spectra of  $\text{ZrO}_2^-$  at different temperatures 300 K (a) and 15 K (b). The photon energy is the same.

### III. RESULTS AND DISCUSSION

Considering the isotope abundance of titanium, the  $\text{Ti}^-/\text{TiH}^-$  ratio for ions with  $m = 48$  is maximum. The signal from  $\text{Ti}^-$  is more notable in the energy spectra for  $m = 48$ . The dominant composition for  $m = 49$  is  $\text{TiH}^-$ , which is chosen for measuring the energy spectra of  $\text{TiH}^-$ . The signals from  $\text{Ti}^-$  can be revealed through the comparison between the energy spectra for  $m = 48$  and that for  $m = 49$ . Figure 3 shows the photoelectron images and binding energy spectra for ions with  $m = 49$  (almost all  $^{48}\text{TiH}^-$ ,  $^{49}\text{Ti}^-$  is barely visible) and  $m = 48$  ( $^{47}\text{TiH}^- + ^{48}\text{Ti}^-$ ) obtained at photon energies  $12\,353.91\text{ cm}^{-1}$  and  $12\,304.39\text{ cm}^{-1}$ , respectively. The VMI imaging voltage is  $-300\text{ V}$ . Three common peaks X1, X2, and A1 appear in the spectra for both  $m = 48$  and  $m = 49$ , suggesting that they are related to the transitions from  $\text{TiH}^-$ . Six narrow peaks labeled as  $a$ - $f$  around  $12\,150\text{ cm}^{-1}$  appear only in the spectrum for  $m = 48$ , as shown in the inset. It is reasonable to assign the six peaks to  $\text{Ti}^-$ . The vertical sticks in the inset represent the calculated intensity. The calculation has considered Wigner's law  $\sigma \propto (eKE)^{3/2}$  for  $p$ -wave detachment. It should be noted that the ion temperature  $800\text{ K}$  is used to estimate the population of excited states in the ion source. The population would not change much during the  $45\text{-ms}$  storage in the ion trap since the transition from excited states down to the ground state is parity-forbidden. Based on the photodetachment selection rules and the energy levels of the neutral Ti

atom, peak  $g$  is related to the transition from the ground state of anion  $\text{Ti}^- (^4\text{F}_{3/2})$  to the ground state of neutral  $\text{Ti} (^3\text{F}_2)$ . Peak  $d$  is assigned to the transition from the ground state  $\text{Ti}^- (^4\text{F}_{3/2})$  to  $\text{Ti} (^3\text{F}_2)$ . Peaks  $a$  and  $e$  represent the transitions from the common initial state  $\text{Ti}^- (^4\text{F}_{5/2})$  to the final states  $\text{Ti} (^3\text{F}_2)$  and  $\text{Ti} (^3\text{F}_3)$ , respectively. Similarly, peaks  $b$  and  $f$  correspond to the transitions from  $\text{Ti}^- (^4\text{F}_{7/2})$  to  $\text{Ti} (^3\text{F}_3)$  and  $\text{Ti} (^3\text{F}_4)$ , respectively. Peak  $c$  corresponds to the transition from  $\text{Ti}^- (^4\text{F}_{9/2})$  to  $\text{Ti} (^3\text{F}_4)$ . The related transitions, energy levels, and anisotropy parameters ( $\beta$ ) to peaks  $a$ - $f$  are summarized in Table I. The measured  $\beta$  values are close to 2, which are consistent with the behavior of  $p$ -wave detachments as expected. The mass spectrum indicates a very weak signal of  $\text{TiH}_2^-$ .  $^{46}\text{TiH}_2^-$  is mixed with  $^{48}\text{Ti}^-$  and  $^{47}\text{TiH}^-$ , similar to the problem we faced in the experiment of Hf.<sup>40</sup> The peak  $\text{M}^*$  is likely due to the contamination of  $^{46}\text{TiH}_2^-$ .

Since the energy levels of neutral atoms are accurately known, the EA measurement is no longer limited to the transition from the ground state of anions to the ground state of neutral atoms. Any transition from the ground state of anions can be used for the EA measurement. This flexibility is important for the elements with an EA value lower than  $0.5\text{ eV}$  because a tunable laser with a narrow linewidth in the infrared range is luxurious. As illustrated in Fig. 4, transition  $d$  is the only transition from the ground state of  $\text{Ti}^-$  in the present work. Therefore, transition  $d$  is selected for measuring the EA of Ti. To accurately determine the binding energy (BE) of peak  $d$ , the

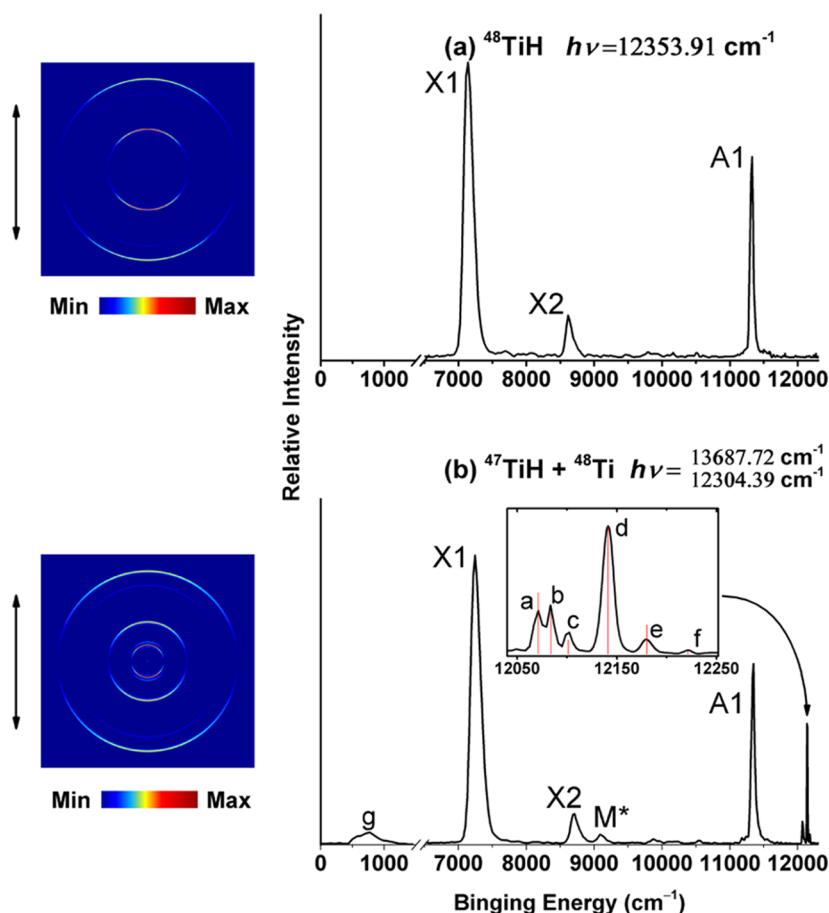


FIG. 3. Photoelectron images and spectra for anions with  $m = 49$  (a) and  $m = 48$  (b) at  $15\text{ K}$ . The inset shows the expanded view of peaks  $a$ - $f$  related to  $\text{Ti}^-$ . Peak  $g$  is obtained using a higher VMI imaging voltage,  $-650\text{ V}$ . The double arrow indicates the polarization of the photodetachment laser. The peaks X1, X2, A1 are related to  $\text{TiH}^-$ .

TABLE I. Measured binding energies and fine structures of  $\text{Ti}^-$ .

Peak	Levels ( $3d^34s \text{ Ti} \leftarrow 3d^34s^2 \text{ Ti}^-$ )	Binding energy ( $\text{cm}^{-1}$ )	Beta
<i>a</i>	$^3F_2 \leftarrow ^4F_{5/2}$	12 070.6(7)	1.7
<i>b</i>	$^3F_3 \leftarrow ^4F_{7/2}$	12 083.5(6)	1.8
<i>c</i>	$^3F_4 \leftarrow ^4F_{9/2}$	12 100.9(12)	1.7
<i>d</i>	$^3F_2 \leftarrow ^4F_{3/2}$	<b>12 141.05(34)<sup>a</sup></b>	<b>1.9</b>
<i>e</i>	$^3F_3 \leftarrow ^4F_{5/2}$	12 179.6(7)	1.7
<i>f</i>	$^3F_4 \leftarrow ^4F_{7/2}$	12 221.2(9)	1.5
Fine structures of $\text{Ti}^-$ ( $\text{cm}^{-1}$ )			
Levels	Extrapolated <sup>b</sup>	Experimental	
$^4F_{5/2} \leftarrow ^4F_{3/2}$	72(7)	70.0(12)	
$^4F_{7/2} \leftarrow ^4F_{3/2}$	171(12)	165.2(13)	
$^4F_{9/2} \leftarrow ^4F_{3/2}$	295(15)	285.2(15)	
Electron affinity	609.29(34) $\text{cm}^{-1}$ or 75.54(4) meV		

<sup>a</sup>Information in bold signifies the selected channel for EA measurement.<sup>b</sup>References 17 and 41.

photon energy  $h\nu$  is varied from 12 194  $\text{cm}^{-1}$  to 12 354  $\text{cm}^{-1}$ , slightly above the threshold, with a step of  $\sim 30 \text{ cm}^{-1}$ . Since  $h\nu = \text{BE} + \alpha r^2$ , the experimental data points are in a line if  $h\nu$  is plotted versus  $r^2$ . As Fig. 5 shows, the intercept of the fitted line is the BE value. The BE value is measured to be 12 141.05  $\text{cm}^{-1}$ . The linear fitting is conducted via the least squares method. The radius  $r$  is obtained via a Gaussian fitting to peak *d*. Figure 6 shows the measured binding energies versus the kinetic energies of photoelectrons. The uncertainty of BE is estimated to be 0.34  $\text{cm}^{-1}$ , which has included the laser linewidth 0.06  $\text{cm}^{-1}$ . The final state of transition *d*,  $\text{Ti}(3d^34s^3F_2)$ , is 11 531.761(2)  $\text{cm}^{-1}$  above the ground state of Ti. Hence, the EA of Ti is determined to be 609.29(34)  $\text{cm}^{-1}$  or

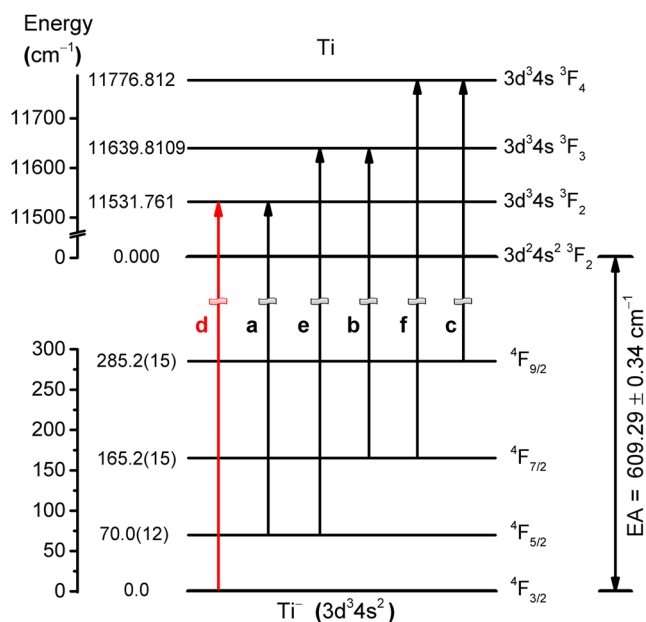


FIG. 4. Energy levels of Ti and  $\text{Ti}^-$  related to the present measurement. The labels of each transition are the indexes of the observed peaks in Fig. 3. The transition *d*,  $\text{Ti}(^3F_2) \leftarrow \text{Ti}^-(^4F_{3/2})$ , is used for the electron affinity measurement.

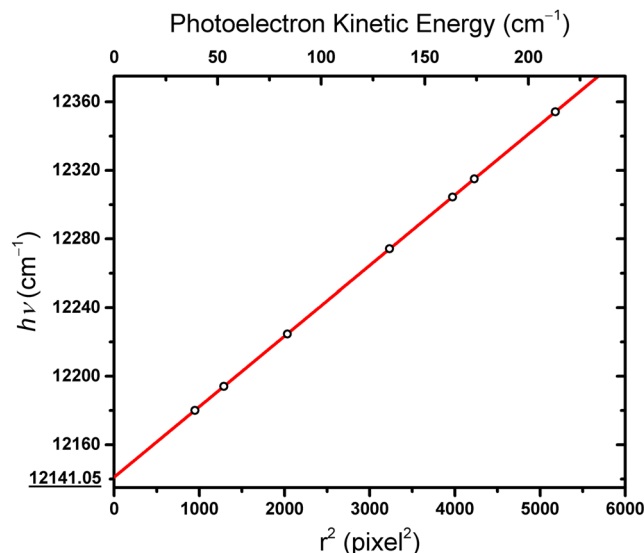


FIG. 5. The photon energy  $h\nu$  versus  $r^2$  for transition *d*. The solid line is the linear least square fitting. The intercept 12 141.05  $\text{cm}^{-1}$  is the binding energy of transition *d*.

75.54(4) meV by subtracting 11 531.76  $\text{cm}^{-1}$  from 12 141.05  $\text{cm}^{-1}$ . Note that 1 eV = 8065.544 005(50)  $\text{cm}^{-1}$ , as recommended by 2014 CODATA.<sup>50</sup> The EA is consistent with that measured by Feigerle *et al.*, but the accuracy is improved by a factor of 350.<sup>17</sup>

The coefficient  $\alpha$  obtained in the linear fitting is used to determine the binding energies of transitions *a*, *b*, *c*, *e*, and *f*. The fine structure splittings of the  $\text{Ti}^-$  can be derived from the binding energies of transitions *a*–*f* according to the relationship illustrated in Fig. 4. For example, the energy difference between transitions *a* and *d* yields the position of the first excited state  $^4F_{5/2}$ . Of course, it can also be determined via the transitions *d* and *e* with the help of the energy level of the neutral atom Ti. The values given by two methods are very close, so an averaged value is used. Finally, the energy levels

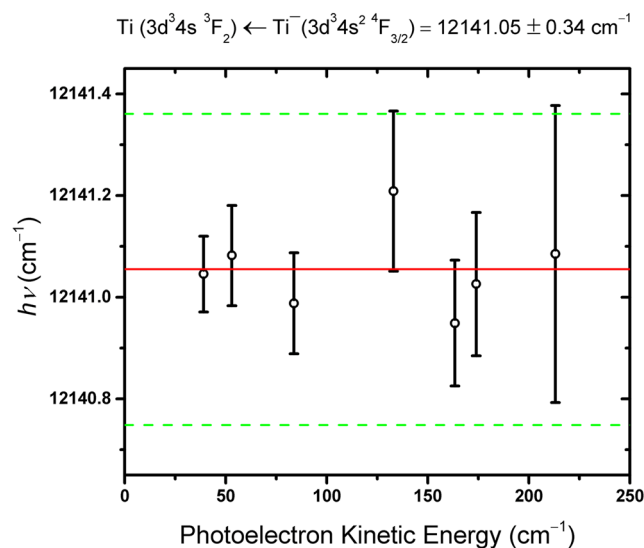


FIG. 6. Binding energy of  $\text{Ti}(^3F_2) \leftarrow \text{Ti}^-(^4F_{3/2})$  transition as a function of the kinetic energy of photoelectrons. The dashed lines indicate the  $\pm 0.34 \text{ cm}^{-1}$  uncertainty.

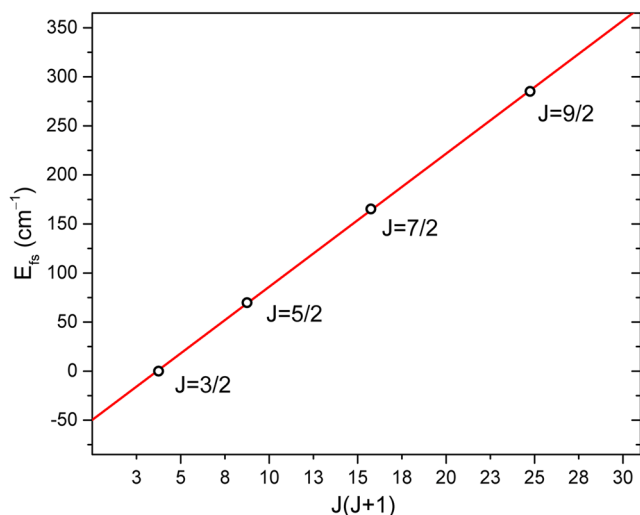


FIG. 7. The spin-orbit energy shift versus  $J(J+1)$  for the fine structures of  $\text{Ti}^-$ .

of the three fine-structure excited states are determined as  $70.0(12)$   $\text{cm}^{-1}$ ,  $165.2(13)$ , and  $285.2(15)$  above the ground state, respectively. The measured values are consistent well with those given by the linear extrapolation. The measured energy levels are summarized in Table I and are illustrated in Fig. 4.

In addition, Ti ( $Z = 22$ ) is not a heavy element, so the relativistic effect is relatively weak. The fine-structure splittings can be described well using Russell-Saunders coupling (LS coupling). The energy shift from the uncoupled state is given by

$$E_J^{(1)} = \frac{1}{2}A[J(J+1) - L(L+1) - S(S+1)], \quad (1)$$

where  $L$ ,  $S$ ,  $J$ ,  $A$  are the orbital quantum number, the spin quantum number, the total angular momentum quantum number, and a coupling constant, respectively. Figure 7 plots the spin-orbit energy shift versus  $J(J+1)$  for the four states of  $\text{Ti}^-$ . It can be seen that the four points are in a straight line. This further confirms our assignments for peak  $a-f$ .

The assignments of peaks X1, X2, A1, and A2 of  $\text{TiH}^-$  are summarized in Table II. The assignment is based on the calculations reported by Burrows *et al.*<sup>51</sup> The ground state of  $\text{TiH}^-$  is  $^3\Phi$  according to our multi-configurational self-consistent field (MCSCF) calculations using the Molpro package.<sup>52</sup> Peak A2, not shown in Fig. 3, is observed at a higher photon energy. The EA of  $\text{TiH}$  is determined to be  $7106(124)$   $\text{cm}^{-1}$ . It should be mentioned that peaks X1 and X2 are notably boarder than a typical molecular peak at the eKE region. The unresolved fine

TABLE II. Peak assignments, positions ( $\text{cm}^{-1}$ ), shifts from the origin ( $\text{cm}^{-1}$ ), and calculated results for  $\text{TiH}^-$  SEVI spectra.

Peak	Electronic	Vibrational	Binding energy ( $\text{cm}^{-1}$ )	Offset ( $\text{cm}^{-1}$ )	Calculated offset <sup>a</sup> ( $\text{cm}^{-1}$ )
X1(EA)	$X^4\Phi \leftarrow X^3\Phi$	0-0	7106(124)	0	
X2	$X^4\Phi \leftarrow X^3\Phi$	1-0	8604(97)	1498	1548.9
A1	$A^4\Delta \leftarrow X^3\Phi$	0-0	11282(46)	4176	4231.0
A2	$A^4\Delta \leftarrow X^3\Phi$	1-0	12792(18)	5686	5630.0

<sup>a</sup>Reference 51.

structures predicted by theoretical calculations may account for the boarder width. As for the theoretical side, we have calculated the EA of  $\text{TiH}$  to be  $6700$   $\text{cm}^{-1}$  using the Gaussian program<sup>53</sup> at the CCSD(T)/aug-cc-pvtz level. Geometry optimization and vibrational zero-point energy corrections are conducted at the B3LYP/aug-cc-pvtz level. The calculated EA value agrees well with the measured value. The vibrational frequency of  $\text{TiH}(^4\Phi)$  is measured to be  $1498(157)$   $\text{cm}^{-1}$ , which is consistent with the reported value  $1385.3$   $\text{cm}^{-1}$  via infrared spectroscopy.<sup>54</sup>

#### IV. CONCLUSION

In conclusion, we obtained the high-resolution photoelectron energy spectra of  $\text{Ti}^-$  and  $\text{TiH}^-$  on our newly built cryo-SEVI apparatus. The electron affinity of Ti was measured to be  $609.29(34)$   $\text{cm}^{-1}$  or  $75.54(4)$  meV. The accuracy was improved by a factor of 350 compared with the previously reported result. In addition, the fine structures of  $\text{Ti}^-$  were well resolved, and its energy levels were determined. It is found that the cryogenically cold ion trap can effectively solve the hydride contamination problem. At present, the electron affinity of most lanthanides is still unknown. We are planning to use this cryo-SEVI method to measure the electron affinities of lanthanides.

#### ACKNOWLEDGMENTS

This work is supported by the National Natural Science Foundation of China (NSFC) (Grant No. 91736102) and the National key R&D program of China (2018YFA0303504).

- <sup>1</sup>M. Grätzel, *Nature* **414**, 338 (2001).
- <sup>2</sup>A. J. Bard, *J. Photochem.* **10**, 59 (1979).
- <sup>3</sup>B. O'Regan and M. Grätzel, *Nature* **353**, 737 (1991).
- <sup>4</sup>G. Phani, G. Tulloch, D. Vittorio, and I. Skryabin, *Renewable Energy* **22**, 303 (2001).
- <sup>5</sup>M. R. Hoffmann, S. T. Martin, W. Choi, and D. W. Bahnemann, *Chem. Rev.* **95**, 69 (1995).
- <sup>6</sup>S. N. Habisreutinger, L. Schmidt-Mende, and J. K. Stolarczyk, *Angew. Chem., Int. Ed.* **52**, 7372 (2013).
- <sup>7</sup>K. Hashimoto, H. Irie, and A. Fujishima, *Jpn. J. Appl. Phys., Part 1* **44**, 8269 (2005).
- <sup>8</sup>A. L. Linsebigler, G. Lu, and J. T. Yates, *Chem. Rev.* **95**, 735 (1995).
- <sup>9</sup>J. A. DeVine, A. Abou Taka, M. C. Babin, M. L. Weichman, H. P. Hratchian, and D. M. Neumark, *J. Chem. Phys.* **148**, 222810 (2018).
- <sup>10</sup>J. B. Kim, M. L. Weichman, and D. M. Neumark, *Phys. Chem. Chem. Phys.* **15**, 20973 (2013).
- <sup>11</sup>E. B. Saloman, *J. Phys. Chem. Ref. Data* **41**, 013101 (2012).
- <sup>12</sup>S. Kobayashi, N. Nishimiya, and M. Suzuki, *J. Phys. Soc. Jpn.* **86**, 104303 (2017).
- <sup>13</sup>P. Vašina, M. Fekete, J. Hnilica, P. Klein, L. Dosoudilová, P. Dvořák, and Z. Navrátil, *Plasma Sources Sci. Technol.* **24**, 065022 (2015).
- <sup>14</sup>X. X. Fu, Z. H. Luo, X. L. Chen, J. M. Li, and C. G. Ning, *J. Chem. Phys.* **145**, 164307 (2016).
- <sup>15</sup>R. C. Bilodeau, M. Scheer, H. K. Haugen, and R. L. Brooks, *Phys. Rev. A* **61**, 012505 (1999).
- <sup>16</sup>M. Scheer, C. A. Brodie, R. C. Bilodeau, and H. K. Haugen, *Phys. Rev. A* **58**, 2051 (1998).
- <sup>17</sup>C. S. Feigerle, R. R. Corderman, S. V. Bobashev, and W. C. Lineberger, *J. Chem. Phys.* **74**, 1580 (1981).
- <sup>18</sup>C. S. Feigerle, R. R. Corderman, and W. C. Lineberger, *J. Chem. Phys.* **74**, 1513 (1981).
- <sup>19</sup>A. Kasdan, E. Herbst, and W. C. Lineberger, *J. Chem. Phys.* **62**, 541 (1975).
- <sup>20</sup>M. Scheer, R. C. Bilodeau, C. A. Brodie, and H. K. Haugen, *Phys. Rev. A* **58**, 2844 (1998).

- <sup>21</sup>E. P. Wigner, *Phys. Rev.* **73**, 1002 (1948).
- <sup>22</sup>X. L. Chen and C. G. Ning, *Phys. Rev. A* **93**, 052508 (2016).
- <sup>23</sup>R. C. Bilodeau, M. Scheer, and H. K. Haugen, *J. Phys. B: at. Mol. Opt. Phys.* **31**, 3885 (1998).
- <sup>24</sup>C. Blondel, W. Chaibi, C. Delsart, C. Drag, F. Goldfarb, and S. Kröger, *Eur. Phys. J. D* **33**, 335 (2005).
- <sup>25</sup>R. J. Peláez, C. Blondel, M. Vandevraye, C. Drag, and C. Delsart, *J. Phys. B: At., Mol. Opt. Phys.* **44**, 195009 (2011).
- <sup>26</sup>M. Vandevraye, C. Drag, and C. Blondel, *Phys. Rev. A* **85**, 612 (2012).
- <sup>27</sup>W. Chaibi, R. J. Peláez, C. Blondel, C. Drag, and C. Delsart, *Eur. Phys. J. D* **58**, 29 (2010).
- <sup>28</sup>T. Carette, C. Drag, O. Scharf, C. Blondel, C. Delsart, C. Froese Fischer, and M. Godefroid, *Phys. Rev. A* **81**, 042522 (2010).
- <sup>29</sup>D. Bresteau, P. Babilotte, C. Drag, and C. Blondel, *J. Phys. B: At., Mol. Opt. Phys.* **48**, 125001 (2015).
- <sup>30</sup>J. B. Kim, M. L. Weichman, T. F. Sjolander, D. M. Neumark, J. K. Os, M. H. Alexander, and D. E. Manolopoulos, *Science* **349**, 510 (2015).
- <sup>31</sup>J. A. DeVine, M. L. Weichman, B. Laws, J. Chang, M. C. Babin, G. Balardi, C. Xie, C. L. Malbon, W. C. Lineberger, D. R. Yarkony, R. W. Field, S. T. Gibson, J. Ma, H. Guo, and D. M. Neumark, *Science* **358**, 336 (2017).
- <sup>32</sup>M. L. Weichman, J. A. DeVine, D. S. Levine, J. B. Kim, and D. M. Neumark, *Proc. Natl. Acad. Sci.* **113**, 1698 (2016).
- <sup>33</sup>E. Garand, J. Zhou, D. E. Manolopoulos, M. H. Alexander, and D. M. Neumark, *Science* **319**, 72 (2008).
- <sup>34</sup>M. L. Weichman and D. M. Neumark, *Annu. Rev. Phys. Chem.* **69**, 101 (2018).
- <sup>35</sup>X. X. Fu, J. M. Li, Z. H. Luo, X. L. Chen, and C. G. Ning, *J. Chem. Phys.* **147**, 064306 (2017).
- <sup>36</sup>X. L. Chen and C. G. Ning, *J. Phys. Chem. Lett.* **8**, 2735 (2017).
- <sup>37</sup>X. L. Chen, Z. H. Luo, J. M. Li, and C. G. Ning, *Sci. Rep.* **6**, 213 (2016).
- <sup>38</sup>X. L. Chen and C. G. Ning, *J. Chem. Phys.* **145**, 084303 (2016).
- <sup>39</sup>Z. H. Luo, X. L. Chen, J. M. Li, and C. G. Ning, *Phys. Rev. A* **93**, 020501(R) (2016).
- <sup>40</sup>R. L. Tang, X. L. Chen, X. X. Fu, H. Wang, and C. G. Ning, *Phys. Rev. A* **98**, 020501(R) (2018).
- <sup>41</sup>T. Andersen, H. K. Haugen, and H. Hotop, *J. Phys. Chem. Ref. Data* **28**, 1511 (1999).
- <sup>42</sup>R. N. Ilin, V. I. Sakharov, and I. T. Serenkov, *Opt. Spectrosc.* **62**, 578 (1987).
- <sup>43</sup>S. R. Liu, H. J. Zhai, M. Castro, and L. S. Wang, *J. Chem. Phys.* **118**, 2108 (2003).
- <sup>44</sup>C. Hock, J. B. Kim, M. L. Weichman, T. I. Yacovitch, and D. M. Neumark, *J. Chem. Phys.* **137**, 244201 (2012).
- <sup>45</sup>X. B. Wang and L. S. Wang, *Rev. Sci. Instrum.* **79**, 073108 (2008).
- <sup>46</sup>W. C. Wiley and I. H. McLaren, *Rev. Sci. Instrum.* **26**, 1150 (1955).
- <sup>47</sup>I. León, Z. Yang, H. T. Liu, and L. S. Wang, *Rev. Sci. Instrum.* **85**, 083106 (2014).
- <sup>48</sup>A. T. J. B. Eppink and D. H. Parker, *Rev. Sci. Instrum.* **68**, 3477 (1997).
- <sup>49</sup>B. Dick, *Phys. Chem. Chem. Phys.* **16**, 570 (2014).
- <sup>50</sup>P. J. Mohr, D. B. Newell, and B. N. Taylor, *Rev. Mod. Phys.* **88**, 035009 (2016).
- <sup>51</sup>A. Burrows, M. Dulick, C. W. Bauschlicher, Jr., P. F. Bernath, R. S. Ram, C. M. Sharp, and J. A. Milsom, *Astrophys. J.* **624**, 988 (2005).
- <sup>52</sup>See <https://www.molpro.net> for Molpro program.
- <sup>53</sup>M. J. Frisch, G. W. Trucks, H. B. Schlegel, G. E. Scuseria, M. A. Robb, J. R. Cheeseman, J. A. Montgomery, Jr., T. Vreven, K. N. Kudin, J. C. Burant, J. M. Millam, S. S. Iyengar, J. Tomasi, V. Barone, B. Mennucci, M. Cossi, G. Scalmani, N. Rega, G. A. Petersson, H. Nakatsuji, M. Hada, M. Ehara, K. Toyota, R. Fukuda, J. Hasegawa, M. Ishida, T. Nakajima, Y. Honda, O. Kitao, H. Nakai, M. Klene, X. Li, J. E. Knox, H. P. Hratchian, J. B. Cross, V. Bakken, C. Adamo, J. Jaramillo, R. Gomperts, R. E. Stratmann, O. Yazyev, A. J. Austin, R. Cammi, C. Pomelli, J. W. Ochterski, P. Y. Ayala, K. Morokuma, G. A. Voth, P. Salvador, J. J. Dannenberg, V. G. Zakrzewski, S. Dapprich, A. D. Daniels, M. C. Strain, O. Farkas, D. K. Malick, A. D. Rabuck, K. Raghavachari, J. B. Foresman, J. V. Ortiz, Q. Cui, A. G. Baboul, S. Clifford, J. Cioslowski, B. B. Stefanov, G. Liu, A. Liashenko, P. Piskorz, I. Komaromi, R. L. Martin, D. J. Fox, T. Keith, M. A. Al-Laham, C. Y. Peng, A. Nanayakkara, M. Challacombe, P. M. W. Gill, B. Johnson, W. Chen, M. W. Wong, C. Gonzalez, and J. A. Pople, Gaussian 03, Revision C.02, Gaussian, Inc., Wallingford, CT, 2004, See <http://www.gaussian.com> for Gaussian program.
- <sup>54</sup>G. V. Chertihin and L. Andrews, *J. Am. Chem. Soc.* **116**, 8322 (1994).